Figure 1. Characteristics of the probands. Number of the probands according to (**A**) diagnostic criteria and (**C**) first symptom. (**B,D,E**) Mean age at diagnosis according to (**B**) diagnostic category or (**D**) first symptom; and (**E**) at onset according to first symptom. CHF, congestive heart failure; CPA, cardiopulmonary arrest. *$P<0.05$, #$P<0.01$.

Figure 2. Number of the patients who fulfilled the criteria for arrhythmogenic right ventricular cardiomyopathy/dysplasia. Red, major criteria; blue, minor criteria; orange, none; light green, gene mutation carriers in major criteria.

Table 2. Desmosomal Gene Mutations Identified in the Present Study

No.	Sex	Age at diagnosis (years)	Category	PKP2 Codon	PKP2 Amino acids	DSP Codon	DSP Amino acids	DSG2 Codon	DSG2 Amino acids	DSC2 Codon	DSC2 Amino acids
1	M	30	Definite	1725–1728dupGATG	R577DfsX5						
2	M	49	Definite								
3	M	16	Definite	1132 C>T	Q378X						
4	F	36	Definite								
5	M	51	Definite								
6	F	15	Definite							394 C>T	R132C
										582 C>G	N194K
										607 C>T	R203C
7	M	64	Definite								
8	F	15	Definite			8269 G>C	D2757H				
9	M	49	Definite			2360 A>G	Y787C				
10	F	47	Definite	2150 C>T	P717L†						
11	M	72	Definite	953 A>C	H318P†						
12	M	45	Definite								
13	M	40	Definite			4741 A>G (H)	K1581E† (H)	1592 T>G	F531C (H)		
14	M	41	Definite	976 G>A (H)	A326T† (H)	593 A>C (H)	Q198P (H)				
15	F	16	Borderline			8455 A>C	M2819L†				
16	M	5	Definite								
17	M	17	Definite	1725–1728dupGATG	R577DfsX5						
18	M	38	Definite								
19	F	25	Borderline								
20	F	63	Possible								
21	M	43	Definite								
22	M	30	Borderline								
23	M	32	Borderline								
24	F	47	Definite								
25	M	70	Definite								
26	F	18	Possible					2780 C>T	P927L#		
27	M	56	Definite	875–890 del	L266QfsX104						
28	F	43	Definite					1481 A>C	D494A† (H)		
29	M	25	Definite	2119 C>T	Q707X						
30	F	63	Definite								
31	M	56	Definite					1481 A>C	D494A†		
32	M	50	Definite			4741 A>G	K1581E†				
33	M	34	Definite	2095 C>T	Q699X			2780 C>T	P927L#		
34	M	62	Definite			1203 G>T	K401N				
35	F	53	Definite	1725–1728dupGATG	R577DfsX5						

†Reported in NCBI SNP database; #identified in the present control cohort. H, homozygous mutation.

healthy Japanese controls.

Age Analysis

The present probands were divided into 2 groups according to age at diagnosis: ≤40 years old (younger group, n=16) and >40 years old (older group, n=19). We also compared the clinical and genetic characteristics between the 2 groups.

Statistical Analysis

All continuous variables are reported as mean±SD. Differences between continuous variables were evaluated using the Wilcoxon rank sum test for 2 groups and 1-way ANOVA for ≥3 groups. Categorical variables were analyzed using chi-square test (for counts ≥5) or Fisher exact test (for counts <5) for 2 groups and Kruskal-Wallis ANOVA rank test for >2 groups. Significance was considered at $P<0.05$.

Results

Clinical Features

Clinical subject characteristics are summarized in **Table 1**. According to the 2010 diagnostic ARVC/D criteria,[18] 29 probands
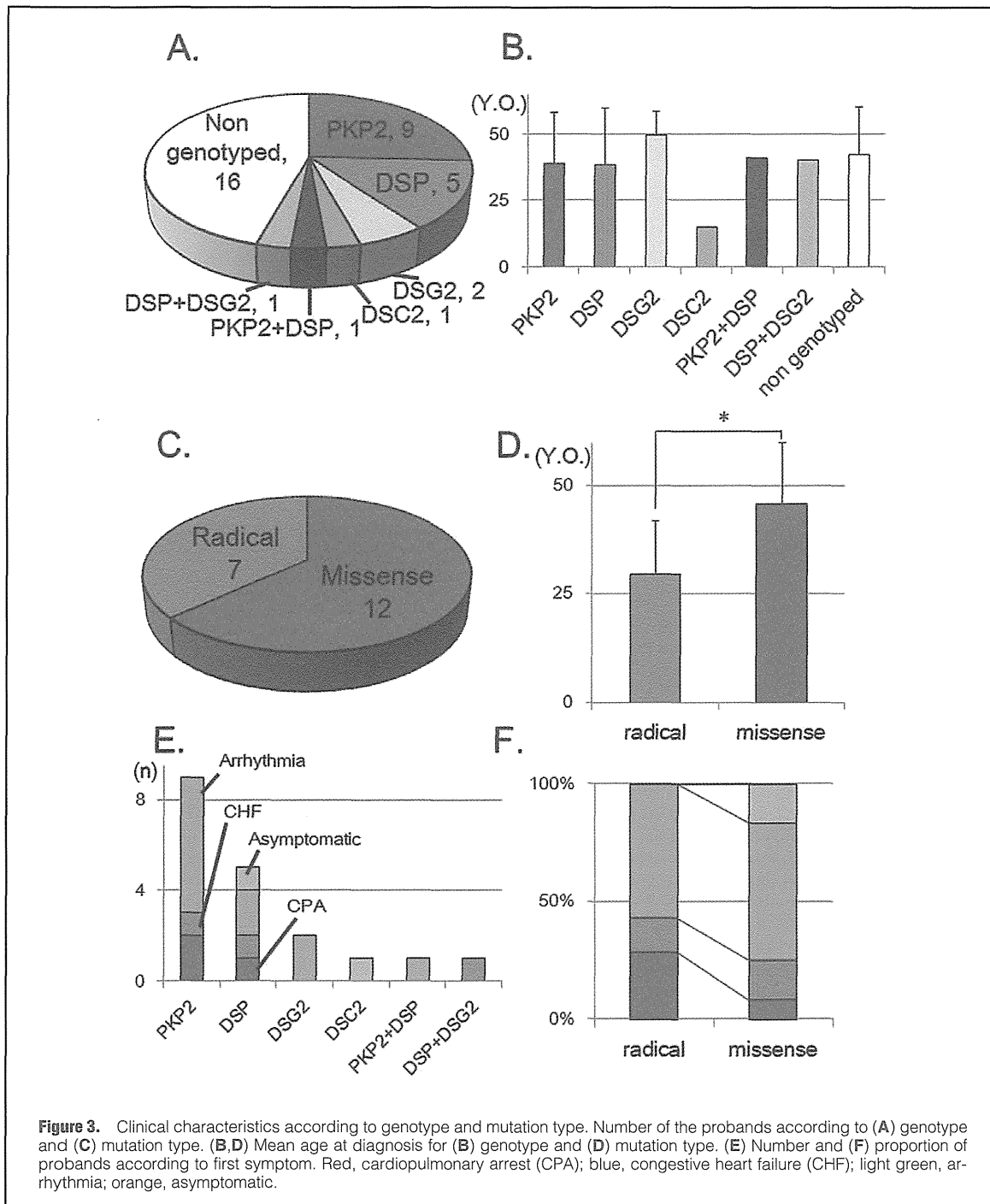
Figure 3. Clinical characteristics according to genotype and mutation type. Number of the probands according to (**A**) genotype and (**C**) mutation type. (**B,D**) Mean age at diagnosis for (**B**) genotype and (**D**) mutation type. (**E**) Number and (**F**) proportion of probands according to first symptom. Red, cardiopulmonary arrest (CPA); blue, congestive heart failure (CHF); light green, arrhythmia; orange, asymptomatic.

(82.9%) were diagnosed as definite, 4 (11.4%) as borderline, and 2 (5.7%) as possible (**Figure 1A**). The mean age at diagnosis was 40.5±17.7 years. They experienced their first symptoms at 38.6±14.8 years, although 2 probands were diagnosed with ARVC/D without symptoms. The asymptomatic probands first consulted doctors due to ECG abnormality, and

were diagnosed with ARVC/D. Mean age at diagnosis in each diagnostic category was not significantly different: 42.5±17.4 years in the definite group, 25.8±7.1 years in the borderline group, and 40.5±31.8 years in the possible group (**Figure 1B**).

Figure 1C summarizes the number of probands according to first symptom, and **Figures 1D,E**, the mean age at diagnosis

Table 3. Subject Characteristics vs. Age at Diagnosis			
	Younger group (n=16)	Older group (n=19)	P-value
Age at onset (years)	24.4±9.5	48.9±7.5	<0.001
Age at diagnosis (years)	24.5±10.2	53.9±9.4	<0.001
Initial manifestation			
Cardiac arrest	5 (31.3)	1 (5.3)	0.073
Arrhythmia	7 (43.8)	14 (73.7)	0.146
Heart failure	2 (12.5)	4 (21.1)	0.666
Asymptomatic	2 (12.5)	0 (0)	0.202
ARVC/D diagnostic criteria			
Definite	11 (68.8)	18 (94.7)	
Borderline	4 (25)	0 (0)	0.333
Possible	1 (6.3)	1 (5.3)	
Desmosomal mutations			
All	9 (54.2)	10 (52.6)	0.899
PKP2	5 (31.3)	4 (21.1)	0.656
PKP2 radical	5 (31.3)	2 (10.5)	0.17
DSP	2 (12.5)	3 (15.8)	1
DSG2	0 (0)	2 (10.5)	1
DSC2	1 (6.3)	0 (0)	0.474
DSP+DSG2	1 (6.3)	0 (0)	0.474
PKP2+DSP	0 (0)	1 (5.3)	1

Data given as mean±SD or n (%). ARVC/D, arrhythmogenic right ventricular cardiomyopathy/dysplasia.

and onset. Probands whose first symptom was cardiopulmonary arrest (CPA) were significantly younger than those whose first symptom was arrhythmia or congestive heart failure. The mean age at onset and diagnosis in the CPA patients were 22.3±15.3 years and 22.7±15.6 years, respectively.

Letters A and I in Table 1 indicate the presence of positive major and minor criteria by the revised task force,[18] respectively. In Table 1, diagnostic criteria are also summed with the result for the diagnostic category. Regarding the RV dysfunction and structural alterations criteria, 24 probands (68.6%) fulfilled major criteria and 1 (2.9%) a minor criterion (Figure 2A). Regarding endocardial biopsy, only 3 probands fulfilled major and 3 minor criteria because tissue characterization from the RV free wall was not available in most cases (Figure 2B). Eight probands (22.9%) fulfilled criteria for major repolarization abnormalities and 4 (11.4%) minor criteria (Figure 2C). Epsilon waves were observed in 5 (14.3%), and 13 (37.1%) had other depolarization abnormalities (Figure 2D). In 33 probands (94.3%), ventricular tachycardia (VT) or frequent premature ventricular contraction (PVCs) was documented; in 13 of them (37.1%), VT with both a superior axis and left bundle-branch morphology was observed (Figure 2E). Only 1 proband (no. 25) had a clear family history of ARVC/D in first-degree relatives, and 19 (54.3%) were found to carry pathogenic mutations in at least 1 gene of desmosomal proteins (M, Table 1) and, therefore, fulfilled family history criteria (Figure 2F).

Genetic Testing
We identified ARVC/D-related gene variants in 19 probands (Table 2). No variants except DSG2-P927L (indicated by #) were identified in the 200 control alleles. Because DSG2-P927L was identified in 1 control as a heterozygote, we classified this variant (probands 26 and 34) as a bystander single-nucleotide polymorphism (SNP). Three of them carried compound or digenic mutations. Mutations indicated by (H)

in Table 2 were homozygous, and those indicated by † are rare variants according to the National Center for Biotechnology Information (NCBI) SNP database.

Figure 3A shows the numbers of carriers of each gene mutation, and Figure 3B the mean age at diagnosis according to genotype, which was not significantly different. PKP2 mutations were identified in 10 probands (28.6%). Seven of them carried radical mutations that caused an inappropriate termination of the protein (Figure 3C). DSP and DSG2 mutations were all missense and were identified in 7 (20.0%) and 3 (8.6%) probands, respectively. One proband (no. 6) carried 3 DSC mutations. The mean age at onset was not significantly different between mutation carriers (39.1±15.5 years) and non-carriers (37.9±14.5 years). Concerning the probands with radical mutations (Figure 3D), onset was significantly younger (29.4±12.4 years) than in those with missense mutations (45.8±14.2 years; P=0.0266). Figure 3E summarizes first symptom according to gene mutation. Three of 6 patients who suffered CPA carried mutations in PKP2 or DSP. Regarding the mutation type (Figure 3F), 2 patients (28.6%) with radical mutations suffered CPA; in contrast, only 1 (8.3%) with a missense mutation did. Two asymptomatic patients carried missense mutations.

Age, and Clinical and Genetic Characteristics
Development of the disease seems to be different between young and older patients, and the mean age at diagnosis in the present cohort was approximately 40 years old. Therefore we divided the present cohort into 2 groups according to this age and compared clinical and genetic characteristics (Table 3). Regarding initial clinical manifestation, 31.3% patients suffered cardiac arrest in the younger group, whereas 5.3% did, in the older group. In contrast, 2 asymptomatic probands belonged to the younger group. Four probands in the younger group were diagnosed as having borderline ARVC/D, whereas none had this in the older group.

Table 4. Clinical and Mutation Characteristics of Family Members

Family no.	Subject no.	Age at diagnosis (years)	Sex	Diagnosis			Mutations
				Major criteria	Minor criteria		Amino acids
3	1	16	M	3	1	Definite	**PKP2 Q378X**
	2	?	M	1		Possible	(–)
	3	?	F	1		Possible	(–)
	4	?	F	1		Possible	(–)
4	1	36	F	2	1	Definite	(–)
	2	11	F	1		Possible	(–)
	3	13	F	1		Possible	(–)
6	1	15	F	2	2	Definite	**DSC R132C N194K R203C**
	2	?	F	1		Possible	DSC N194K R203C
	3	12	M	1		Possible	(–)
13	1	40	M	2	2	Definite	**DSP K1581E*(H) DSG2 F531C**
	2	76	M	1		Possible	DSP K1581E* DSG2 F531C
	3	66	F	1		Possible	DSP K1581E*
17	1	17	M	3	1	Definite	**PKP2 R577DfsX5**
	2	20	M	3		Definite	PKP2 R577DfsX5
18	1	38	M	1	2	Definite	(–)
	2	7	M	1		Possible	(–)
28	1	43	F	3		Definite	**DSG2 D494A***
	2	56	M	2		Definite	DSG2 D494A*
	3	23	M	1		Possible	DSG2 D494A*
	4	14	F	1		Possible	DSG2 D494A*
31	1	56	M	2	2	Definite	**DSG2 D494A***
	2	61	F	2	1	Definite	DSG2 D494A*
	3	26	F	1		Possible	(–)

Bold, Proband. *Reported in NCBI SNP database.

Desmosomal gene mutations were identified in 9 probands from the younger group and in 10 from the older group. There was no difference in the number of mutation carriers of the respective genes. Five probands from each group carried *PKP2* mutations, but the number of radical *PKP2* mutation carriers was higher in the younger (n=5) than the older (n=2) group.

Family Members

We examined 16 family members from 8 families, and identified desmosomal gene mutations in 8 members from 6 families (Table 4). Only 3 of them satisfied the diagnostic criteria for definite ARVC/D and they were all found to have desmosomal gene mutations. A 20-year-old man with a definite diagnosis (subject 17-2) remained asymptomatic without treatment. In contrast, 2 other family members with a definite diagnosis (28-2 and 31-2) were a 56-year-old man and a 61-year-old woman, and both were symptomatic and receiving treatment. The remaining family members were diagnosed in the possible category because first-degree relatives fulfilled the major criteria of family history.

Discussion

In this study, we first performed a comprehensive examination of 35 Japanese ARVC/D patients and their 16 family members. Furthermore, we analyzed the age-dependent clinical and genetic features of the ARVC/D patients.

Age-Dependent Features

In the clinical course of ARVC/D, it is well-known that patients become symptomatic at around 40.[15,16] Because the disease displays a dominant or recessive inheritance trait, we can examine the family members after the diagnosis of the probands. Advances in molecular genetics facilitated the early detection of ARVC/D before disease onset not only for possible probands, but also their family members. In contrast, however, sporadic cases were rarely diagnosed before onset. As described here, 5 young patients suffered from cardiac arrest as the first symptom. Also, in the present cohort, 2 young patients were diagnosed before onset of symptoms due to ECG abnormalities recorded in a health check-up at high school. One had frequent PVCs and another had T-wave inversion in the right precordial leads.

Corrado et al described the age dependence of the disease with regard to the clinicopathology.[21] They analyzed 42 whole hearts of patients with a pathologic diagnosis of ARVC/D at postmortem examination or after heart transplantation. According to the left ventricular (LV) involvement, the patients were classified into 3 groups. Consequently, they reported that the group with LV involvement was significantly older than the others and had highly developed heart failure. This agrees with the present finding of the patients whose onset was heart failure being older than those who developed cardiac arrest. Concerning the unexpected sudden cardiac death, 200 of 1,930 autopsy subjects were diagnosed as having ARVC/D.[22] In that report, there was a gradual increase of sudden cardiac death until the late 30s, followed by a progressive decrease.

In a recent study involving 53 pediatric ARVC/D patients with desmosomal mutations,[17] only 40% of mutation carriers fulfilled the diagnostic criteria. The frequency of ECG abnormality in genotyped patients, however, was significantly higher in probands than in family members; 12 of 13 probands in that study had ECG abnormality.[17] Taken together, ECG in adolescence would be effective for the early diagnosis of ARVC/D, as well as the prevention of sudden cardiac death. In Japan, ECG is obligatory in schools at the age of 6, 12, and 15 years. Therefore, we can identify abnormal ECG carriers, and further examine their cardiac function to prevent unexpected cardiac sudden death.

Although there was no age dependence in each gene mutation carrier, carriers with *PKP2* radical mutations developed the disease at a significantly younger age than other mutation carriers (Figure 3D). This implies that nonsense or frameshift mutations may cause severer phenotypes and the early onset of ARVC/D, because multiple desmosomal mutations cause earlier onset and more severe phenotype.[16,23] In Table 3, we could not identify the clear clinical and genetic differences between younger and older groups, but we should bear in mind that the onset in the younger ARVC/D patients might be CPA, as shown in Figures 1D,E.

Desmosomal Mutations in Japan

Kapplinger et al reported desmosomal gene mutations identified in healthy controls in comparison with ARVC/D patients.[24] They reported that missense mutations in *DSP* and *DSG2* were frequently identified in non-Caucasian controls. Concerning the desmosomal variant, Fressart et al used software to distinguish whether the variants were disease-causing mutations or genetic variants of unknown significance.[16] In the present cohort, we identified 2 *DSG2*-P927L carriers in the healthy controls. Also, 5 desmosomal variants we found were reported in the NCBI SNP database. It was, however, difficult to distinguish whether the variants were benign or not, because the healthy controls might develop the disease at a later date. Concerning the family members, only 3 of 8 with gene mutations fulfilled the criteria for definite ARVC/D. Originally, the penetrance of the disease with *PKP2* mutations was reported to be very low.[3,8,25] As the reason for low penetrance, additional genetic or environmental factors, including age, might affect the onset of the disease. Therefore, we need to perform careful follow-up of the genotyped family members to elucidate the effect of the variants on the progression of the disease, especially in young carriers.

Study Limitations

The number of ARVC/D patients in the present study was limited to 35, and this number was smaller than in other studies reported from Europe and the USA. Because we did not screen for *JUP*, the present mutation-negative patients may have carried mutations of *JUP*.

Conclusions

In Japan, as reported in Western countries, *PKP2* mutations are the major cause of ARVC/D among desmosomal genes. In young patients, fatal arrhythmias and cardiac arrest are sometimes the first symptom; therefore, the identification of genetically affected family members, especially those with *PKP2* mutations causing a premature stop codon, is indispensable for preventing sudden death.

References

1. Basso C, Corrado D, Marcus FI, Nava A, Thiene G. Arrhythmogenic right ventricular cardiomyopathy. *Lancet* 2009; **373:** 1289–1300.
2. Rampazzo A, Nava A, Malacrida S, Beffagna G, Bauce B, Rossi V, et al. Mutation in human desmoplakin domain binding to plakoglobin causes a dominant form of arrhythmogenic right ventricular cardiomyopathy. *Am J Hum Genet* 2002; **71:** 1200–1206.
3. Gerull B, Heuser A, Wichter T, Paul M, Basson CT, McDermott DA, et al. Mutations in the desmosomal protein plakophilin-2 are common in arrhythmogenic right ventricular cardiomyopathy. *Nat Genet* 2004; **36:** 1162–1164.
4. Pilichou K, Nava A, Basso C, Beffagna G, Bauce B, Lorenzon A, et al. Mutations in desmoglein-2 gene are associated with arrhythmogenic right ventricular cardiomyopathy. *Circulation* 2006; **113:** 1171–1179.
5. Syrris P, Ward D, Evans A, Asimaki A, Gandjbakhch E, Sen-Chowdhry S, et al. Arrhythmogenic right ventricular dysplasia/cardiomyopathy associated with mutations in the desmosomal gene desmocollin-2. *Am J Hum Genet* 2006; **79:** 978–984.
6. Asimaki A, Syrris P, Wichter T, Matthias P, Saffitz JE, McKenna WJ. A novel dominant mutation in plakoglobin causes arrhythmogenic right ventricular cardiomyopathy. *Am J Hum Genet* 2007; **81:** 964–973.
7. Klauke B, Kossmann S, Gaertner A, Brand K, Stork I, Brodehl A, et al. De novo desmin-mutation N116S is associated with arrhythmogenic right ventricular cardiomyopathy. *Hum Mol Genet* 2010; **19:** 4595–4607.
8. Xu T, Yang Z, Vatta M, Rampazzo A, Beffagna G, Pilichou K, et al. Compound and digenic heterozygosity contributes to arrhythmogenic right ventricular cardiomyopathy. *J Am Coll Cardiol* 2010; **55:** 587–597.
9. Taylor M, Graw S, Sinagra G, Barnes C, Slavov D, Brun F, et al. Genetic variation in titin in arrhythmogenic right ventricular cardiomyopathy-overlap syndromes. *Circulation* 2011; **124:** 876–885.
10. Nagaoka I, Matsui K, Ueyama T, Kanemoto M, Wu J, Shimizu A, et al. Novel mutation of plakophilin-2 associated with arrhythmogenic right ventricular cardiomyopathy. *Circ J* 2006; **70:** 933–935.
11. Nakajima T, Kaneko Y, Irie T, Takahashi R, Kato T, Iijima T, et al. Compound and digenic heterozygosity in desmosome genes as a cause of arrhythmogenic right ventricular cardiomyopathy in Japanese patients. *Circ J* 2012; **76:** 737–743.
12. Qiu X, Liu W, Hu D, Zhu T, Li C, Li L, et al. Mutations of plakophilin-2 in Chinese with arrhythmogenic right ventricular dysplasia/cardiomyopathy. *Am J Cardiol* 2009; **103:** 1439–1444.
13. Wu SL, Wang PN, Hou YS, Zhang XC, Shan ZX, Yu XY, et al. Mutation of plakophilin-2 gene in arrhythmogenic right ventricular cardiomyopathy. *Chin Med J (Engl)* 2009; **122:** 403–407.
14. Zhang M, Tavora F, Oliveira JB, Li L, Franco M, Fowler D, et al. PKP2 mutations in sudden death from arrhythmogenic right ventricular cardiomyopathy (ARVC) and sudden unexpected death with negative autopsy (SUDNA). *Circ J* 2012; **76:** 189–194.
15. den Haan AD, Tan BY, Zikusoka MN, Llado LI, Jain R, Daly A, et al. Comprehensive desmosome mutation analysis in North Americans with arrhythmogenic right ventricular dysplasia/cardiomyopathy. *Circ Cardiovasc Genet* 2009; **2:** 428–435.
16. Fressart V, Duthoit G, Donal E, Probst V, Deharo JC, Chevalier P, et al. Desmosomal gene analysis in arrhythmogenic right ventricular dysplasia/cardiomyopathy: Spectrum of mutations and clinical impact in practice. *Europace* 2010; **12:** 861–868.
17. Bauce B, Rampazzo A, Basso C, Mazzotti E, Rigato I, Steriotis A, et al. Clinical phenotype and diagnosis of arrhythmogenic right ventricular cardiomyopathy in pediatric patients carrying desmosomal gene mutations. *Heart Rhythm* 2011; **8:** 1686–1695.
18. Marcus FI, McKenna WJ, Sherrill D, Basso C, Bauce B, Bluemke DA, et al. Diagnosis of arrhythmogenic right ventricular cardiomyopathy/dysplasia: Proposed modification of the task force criteria.

Circulation 2010; **121**: 1533–1541.

19. Ohno S, Zankov DP, Yoshida H, Tsuji K, Makiyama T, Itoh H, et al. N- and C-terminal KCNE1 mutations cause distinct phenotypes of long QT syndrome. *Heart Rhythm* 2007; **4**: 332–340.

20. Quarta G, Syrris P, Ashworth M, Jenkins S, Zuborne Alapi K, Morgan J, et al. Mutations in the Lamin A/C gene mimic arrhythmogenic right ventricular cardiomyopathy. *Eur Heart J* 2012; **33**: 1128–1136.

21. Corrado D, Basso C, Thiene G, McKenna WJ, Davies MJ, Fontaliran F, et al. Spectrum of clinicopathologic manifestations of arrhythmogenic right ventricular cardiomyopathy/dysplasia: A multicenter study. *J Am Coll Cardiol* 1997; **30**: 1512–1520.

22. Tabib A, Loire R, Chalabreysse L, Meyronnet D, Miras A, Malicier D, et al. Circumstances of death and gross and microscopic observations in a series of 200 cases of sudden death associated with arrhythmo-genic right ventricular cardiomyopathy and/or dysplasia. *Circulation* 2003; **108**: 3000–3005.

23. Bauce B, Nava A, Beffagna G, Basso C, Lorenzon A, Smaniotto G, et al. Multiple mutations in desmosomal proteins encoding genes in arrhythmogenic right ventricular cardiomyopathy/dysplasia. *Heart Rhythm* 2010; **7**: 22–29.

24. Kapplinger JD, Landstrom AP, Salisbury BA, Callis TE, Pollevick GD, Tester DJ, et al. Distinguishing arrhythmogenic right ventricular cardiomyopathy/dysplasia-associated mutations from background genetic noise. *J Am Coll Cardiol* 2011; **57**: 2317–2327.

25. Dalal D, James C, Devanagondi R, Tichnell C, Tucker A, Prakasa K, et al. Penetrance of mutations in plakophilin-2 among families with arrhythmogenic right ventricular dysplasia/cardiomyopathy. *J Am Coll Cardiol* 2006; **48**: 1416–1424.

Ultrastructural Maturation of Human-Induced Pluripotent Stem Cell-Derived Cardiomyocytes in a Long-Term Culture

Tsukasa Kamakura, MD; Takeru Makiyama, MD, PhD; Kenichi Sasaki, MD;
Yoshinori Yoshida, MD, PhD; Yimin Wuriyanghai; Jiarong Chen;
Tetsuhisa Hattori, MD, PhD; Seiko Ohno, MD, PhD; Toru Kita, MD, PhD;
Minoru Horie, MD, PhD; Shinya Yamanaka, MD, PhD; Takeshi Kimura, MD, PhD

Background: In the short- to mid-term, cardiomyocytes generated from human-induced pluripotent stem cells (hiPSC-CMs) have been reported to be less mature than those of adult hearts. However, the maturation process in a long-term culture remains unknown.

Methods and Results: A hiPSC clone generated from a healthy control was differentiated into CMs through embryoid body (EB) formation. The ultrastructural characteristics and gene expressions of spontaneously contracting EBs were analyzed through 1-year of culture after cardiac differentiation was initiated. The 14-day-old EBs contained a low number of myofibrils, which lacked alignment, and immature high-density Z-bands lacking A-, H-, I-, and M-bands. Through the long-term culture up to 180 days, the myofibrils became more tightly packed and formed parallel arrays accompanied by the appearance of mature Z-, A-, H-, and I-bands, but not M-bands. Notably, M-bands were finally detected in 360-day-old EBs. The expression levels of the M-band-specific genes in hiPSC-CMs remained lower in comparison with those in the adult heart. Immunocytochemistry indicated increasing number of MLC2v-positive/MLC2a-negative cells with decreasing number of MLC2v/MLC2a double-positive cells, indicating maturing of ventricular-type CMs.

Conclusions: The structural maturation process of hiPSC-CMs through 1-year of culture revealed ultrastructural sarcomeric changes accompanied by delayed formation of M-bands. Our study provides new insight into the maturation process of hiPSC-CMs.

Key Words: Cardiomyocytes; Induced pluripotent stem cells; Ultrastructure

Induced pluripotent stem cells (iPSC) can differentiate into functional cardiomyocytes (CMs), and are a powerful model for regenerative therapy and investigating the mechanisms underlying inherited cardiac diseases.[1–5] Although several studies have shown that iPSC-derived CMs (iPSC-CMs) have molecular, structural and functional properties resembling those of adult CMs,[6–9] they have proved to be less mature than adult and fetal CMs.[10–12] Thus, there is limited information about the electrophysiological and biochemical properties of iPSC-CMs, and the ultrastructural maturation process has not been investigated fully.

The ultrastructural features of human iPSC-CMs (hiPSC-CMs) at around 30 days after cardiac differentiation have been described as being similar to those of adult CMs showing myofibrillar bundles with transverse Z-bands.[4,13,14] However, in those reports, hiPSC-CMs still remain embryonic in phenotype, lacking a mature sarcomeric structure with M-bands and a variable degree of myofibrillar organization. It is unknown whether hiPSC-CMs can develop the adult CM-like ultrastructure in vitro. Immaturity of the hiPSC-CMs may hamper their application for studying cardiac diseases, drug development, and regenerative medicine, and could affect functional properties and drug responses in vitro and increase the risk of abnormal growth in vivo. Therefore, it is crucial to elucidate the
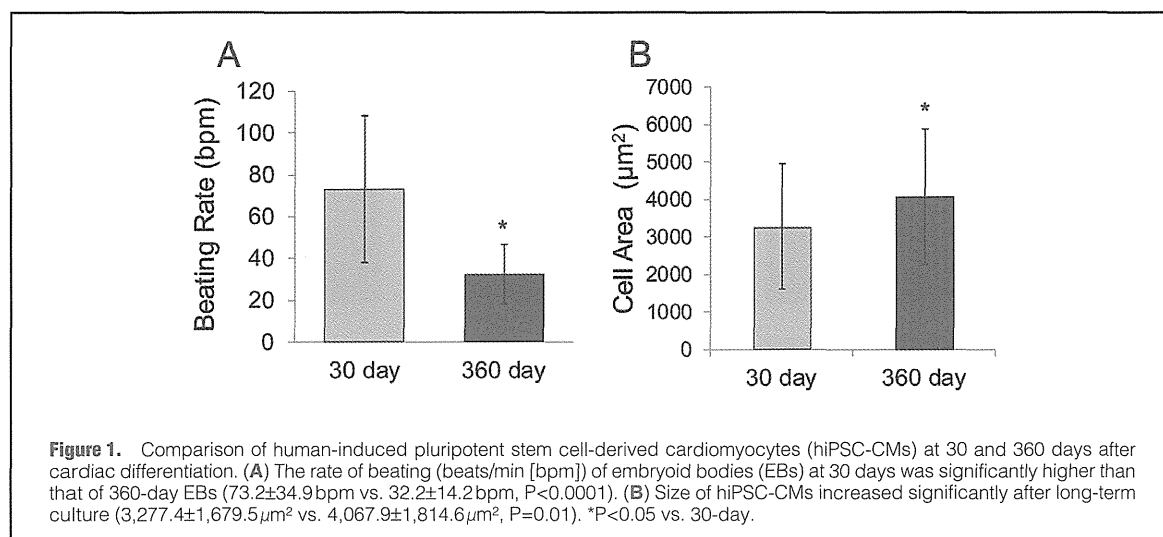
Figure 1. Comparison of human-induced pluripotent stem cell-derived cardiomyocytes (hiPSC-CMs) at 30 and 360 days after cardiac differentiation. (A) The rate of beating (beats/min [bpm]) of embryoid bodies (EBs) at 30 days was significantly higher than that of 360-day EBs (73.2±34.9 bpm vs. 32.2±14.2 bpm, P<0.0001). (B) Size of hiPSC-CMs increased significantly after long-term culture (3,277.4±1,679.5 μm² vs. 4,067.9±1,814.6 μm², P=0.01). *P<0.05 vs. 30-day.

maturation process and establish a protocol for creating homogeneous mature iPSC-CMs.

In this study, we investigated the ultrastructural, immunocytological, and gene expression changes of hiPSC-CMs in a long-term 2D culture. Here, we first report that mature sarcomeric structures with M-bands were detected only in 360-day hiPSC-CMs, which might be associated with lower expression levels of M-band-specific proteins compared with adult heart cells.

Methods

Culture of hiPSC and CM Differentiation

The hiPSC line 201B7 was retrovirally transfected with Oct3/4, SOX-2, Klf4, and c-Myc.[1,9] These lines displayed all the defining parameters[1] and the hiPSCs were maintained as described.[15]

We differentiated hiPSC-CMs as embryoid bodies (EBs).[16,17] In brief, hiPSCs aggregated to form EBs, and were cultured in suspension for 8 days. On day 8, the EBs were plated onto fibronectin-coated dishes and for the first 20 days, we followed the protocol as described previously.[16,17] Cultures were maintained in a 5% CO_2, 5% O_2, 90% N_2 environment for the first 12 days and then transferred into a 5% CO_2/air environment for the remainder of the culture period. At 20 days after cardiac differentiation, EBs were maintained in culture DMEM/F12 supplemented with 2% fetal bovine serum, 2 mmol/L L-glutamine, 0.1 mmol/L non-essential amino acids, 0.1 mmol/L β-mercaptoethanol, 50 U/ml penicillin, and 50 μg/ml streptomycin.[3] The medium was renewed every 2–3 days.

Immunocytochemistry

For immunostaining, single cells were isolated from microdissected 30- and 360-day-old beating EBs using collagenase B (Roche) and trypsin EDTA (Nacalai Tesque). The cells were plated onto fibronectin-coated dishes for 3 days to allow attachment. The cells were fixed in 4% paraformaldehyde and permeabilized in 0.2% Triton X-100 (Nacalai Tesque). The samples were stained with the following primary antibodies: rabbit polyclonal anti-cardiac troponin I (cTnI) (1:200; Santa Cruz), mouse monoclonal anti-myosin light chain 2a (MLC2a) (1:200; Synaptic Systems), rabbit polyclonal anti-myosin light

chain 2v (MLC2v) (1:100; Proteintech Group), mouse monoclonal anti-βIII tubulin (1:100, Promega), mouse monoclonal anti-fibroblast (1:100, Acris Antibodies), and mouse monoclonal anti-human smooth muscle actin (1:100, Dako). We used the appropriate secondary antibodies: donkey anti-rabbit Alexafluor 594 (1:500, Invitrogen) and donkey anti-mouse Alexafluor 488 (1:500, Invitrogen). The nuclei were stained with DAPI (1:2000, Wako). The specimens were observed under a fluorescence microscope, Biozero BZ-9000 (Keyence), and the areas of cTnI-positive cells were calculated using a BZ-II analyzer (Keyence).

Transmission Electron Microscopy (TEM)

TEM was performed on 14-, 30-, 60-, 90-, 180-, and 360-day old EBs derived from hiPSC-CMs. EBs were microdissected and fixed for 1 h in 2% glutaraldehyde at 4°C in phosphate-buffered saline (PBS). All sections were treated with OsO_4 (1% for 1 min, and 0.5% for 20 min at 4°C) in PBS, dehydrated in ethanol and propylene oxide, and embedded in Luveak 812 (Nacalai Tesque). Ultrathin sections were cut with an ultramicrotome (Leica, Heidelberg, Germany) and observed with TEM (H-7650; Hitachi). All stages of EBs were examined in triplicate.

Analysis of mRNA Expression by Real-Time Quantitative Polymerase Chain Reaction (qPCR)

Total RNA was isolated using TRIzol Reagent (Invitrogen) from 20 to 30 EBs microdissected from 30-, 90-, 180-, and 360-day-old hiPSC-CMs, and treated with TURBO DNA-free Kit (Applied Biosystems). Total RNA from human heart tissue (left ventricle, left atrium, and fetal heart) was also reverse transcribed into complementary DNA (cDNA) for comparison. cDNA was synthesized from 1 μg of total RNA, in a total volume of 20 μl, using oligo (dT)18 primer with Transcriptor First Strand cDNA Synthesis Kit (Roche). The PCR-related primers are detailed in Table S1. The real-time qPCR was performed using power SYBR Green PCR Master Mix (Applied Biosystems) for 6 samples. The expression of genes of interest was normalized to that of GAPDH. Relative quantification was calculated according to the ΔΔCt method. The changes in gene expression levels were compared with those of hiPSC-
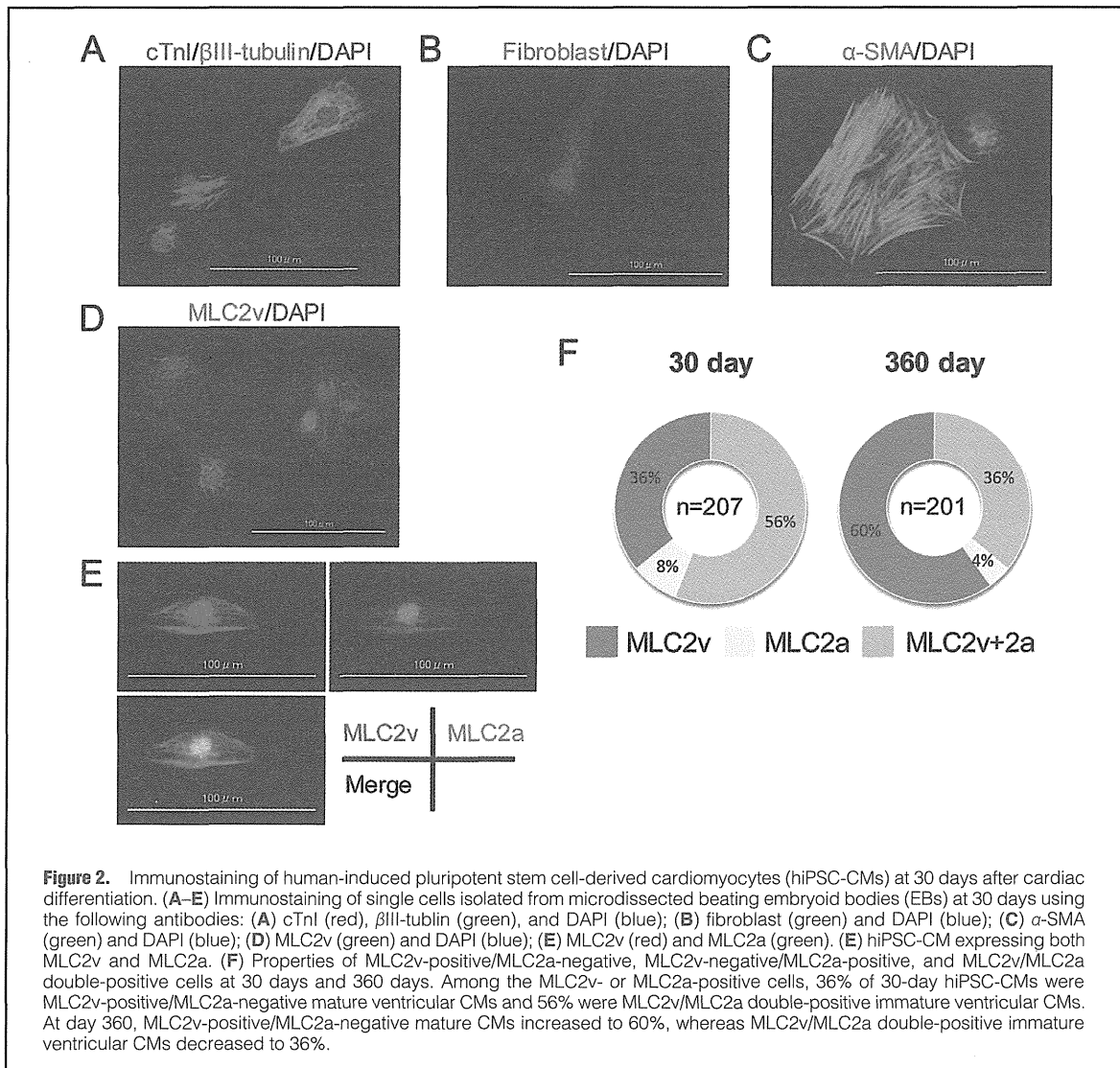
Figure 2. Immunostaining of human-induced pluripotent stem cell-derived cardiomyocytes (hiPSC-CMs) at 30 days after cardiac differentiation. (A–E) Immunostaining of single cells isolated from microdissected beating embryoid bodies (EBs) at 30 days using the following antibodies: (A) cTnI (red), βIII-tublin (green), and DAPI (blue); (B) fibroblast (green) and DAPI (blue); (C) α-SMA (green) and DAPI (blue); (D) MLC2v (green) and DAPI (blue); (E) MLC2v (red) and MLC2a (green). (E) hiPSC-CM expressing both MLC2v and MLC2a. (F) Properties of MLC2v-positive/MLC2a-negative, MLC2v-negative/MLC2a-positive, and MLC2v/MLC2a double-positive cells at 30 days and 360 days. Among the MLC2v- or MLC2a-positive cells, 36% of 30-day hiPSC-CMs were MLC2v-positive/MLC2a-negative mature ventricular CMs and 56% were MLC2v/MLC2a double-positive immature ventricular CMs. At day 360, MLC2v-positive/MLC2a-negative mature CMs increased to 60%, whereas MLC2v/MLC2a double-positive immature ventricular CMs decreased to 36%.

CMs at 30-day differentiation. The fold change is expressed as mean±SEM.

Statistical Analysis

All values are presented as mean±SEM. Statistical significance was evaluated by Student's t-test for 2 groups or 1-way analysis of variance followed by Tukey test for comparisons of multiple groups. Differences with P<0.05 were considered statistically significant.

Results

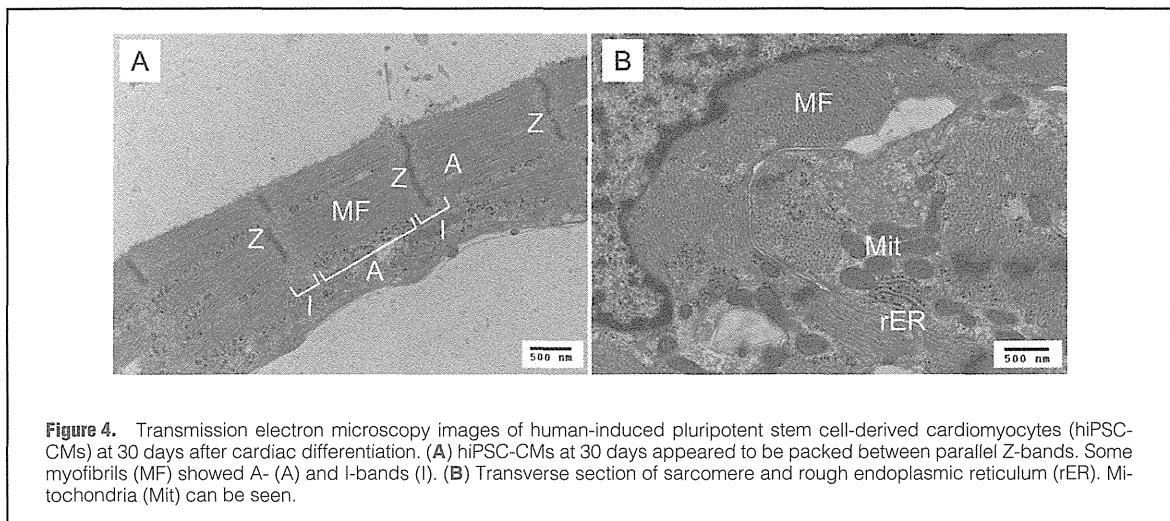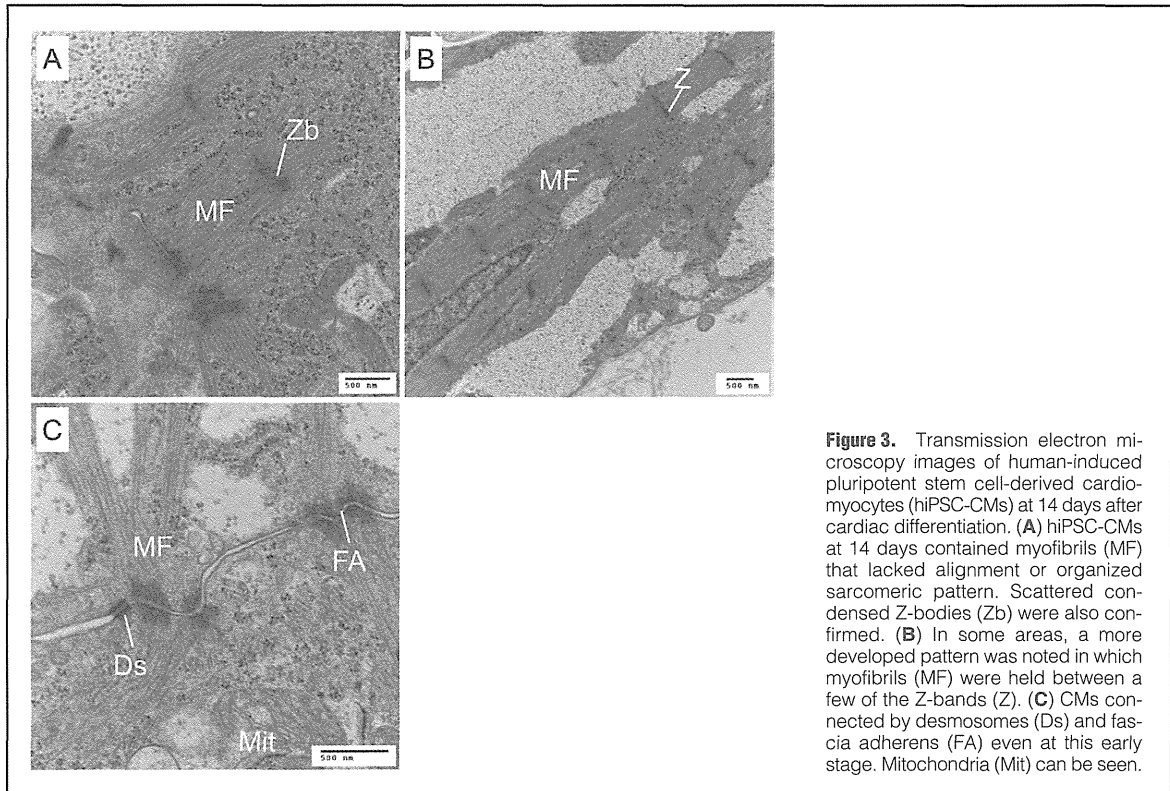### Long-Term Maintenance of hiPSC-CMs

Areas of spontaneous beating became visible as early as day 8 after differentiation, and kept beating for more than 360 days (**Movie S1**). The beating rate of 30-day-old EBs (n=42) was significantly higher than that of 360-day-old EBs (n=41; 73.2± 34.9 beats/min vs. 32.2±14.2 beats/min, P<0.0001) (**Figure 1A**).

The size of dispersed hiPSC-CMs increased significantly after long-term culture as measured by their cell area (3,277.4± 1,679.5 μm^2 vs. 4,067.9±1,814.6 μm^2, P=0.01) (**Figure 1B**).

Immunostaining Analysis of Beating EBs at 30 and 360 Days After Cardiac Differentiation

Immunostaining of single cells isolated by microdissected beating EBs detected cells positive not only for cTnI, MLC2v, and MLC2a, but also βIII-tubulin, fibroblasts, and α-SMA, suggesting the existence of neural cells, fibroblast-like cells, and vascular smooth muscle cells in the beating EBs as well as CMs (**Figures 2A–E**).

Among randomly selected single cells isolated from 30-(n=213) and 360-day-old (n=191) beating EBs, 61% and 64%, respectively, were positive for cTnI. Double immunostaining with anti-MLC2v and anti-MLC2a antibodies revealed that among the MLC2v- or MLC2a-positive cells, 36% were MLC2v-positive/MLC2a-negative, 8% were MLC2v-negative/
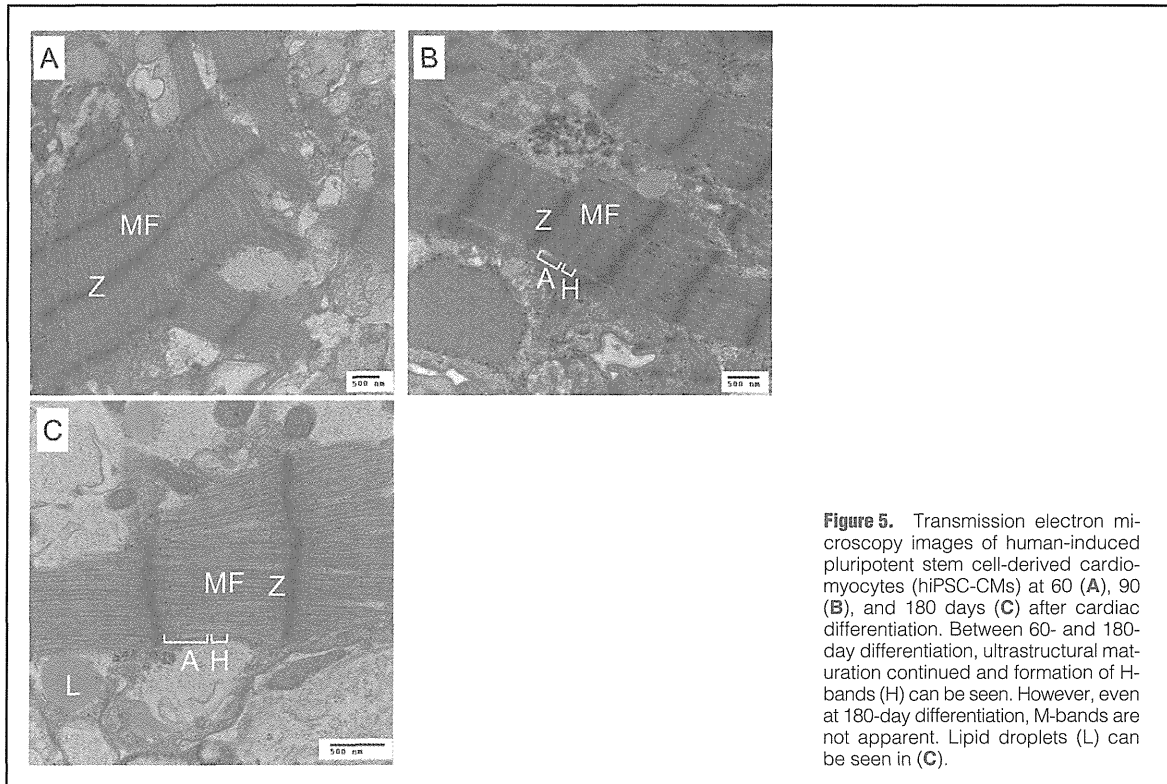
Figure 3. Transmission electron microscopy images of human-induced pluripotent stem cell-derived cardiomyocytes (hiPSC-CMs) at 14 days after cardiac differentiation. (**A**) hiPSC-CMs at 14 days contained myofibrils (MF) that lacked alignment or organized sarcomeric pattern. Scattered condensed Z-bodies (Zb) were also confirmed. (**B**) In some areas, a more developed pattern was noted in which myofibrils (MF) were held between a few of the Z-bands (Z). (**C**) CMs connected by desmosomes (Ds) and fascia adherens (FA) even at this early stage. Mitochondria (Mit) can be seen.

Figure 4. Transmission electron microscopy images of human-induced pluripotent stem cell-derived cardiomyocytes (hiPSC-CMs) at 30 days after cardiac differentiation. (**A**) hiPSC-CMs at 30 days appeared to be packed between parallel Z-bands. Some myofibrils (MF) showed A- (A) and I-bands (I). (**B**) Transverse section of sarcomere and rough endoplasmic reticulum (rER). Mitochondria (Mit) can be seen.

MLC2a-positive, and 56% were MLC2v/MLC2a double-positive CMs at 30-day differentiation. By day 360, MLC2v-positive/MLC2a-negative CMs increased to 60%, whereas MLC2v/MLC2a double-positive immature ventricular CMs decreased to 36% (**Figure 2F**).

Ultrastructural Analysis of hiPSC-CMs at 14-, 30-, 60-, 90-, 180-, and 360-Day Differentiation

hiPSC-CMs at 14-day differentiation contained myofibrils that lacked alignment or organized sarcomeric pattern, and were distributed diffusely in the cytoplasm in a disorganized fashion. Scattered patterns of condensed Z-bodies were also confirmed. However, in some areas, a more developed pattern was

Figure 5. Transmission electron microscopy images of human-induced pluripotent stem cell-derived cardiomyocytes (hiPSC-CMs) at 60 (**A**), 90 (**B**), and 180 days (**C**) after cardiac differentiation. Between 60- and 180-day differentiation, ultrastructural maturation continued and formation of H-bands (H) can be seen. However, even at 180-day differentiation, M-bands are not apparent. Lipid droplets (L) can be seen in (**C**).
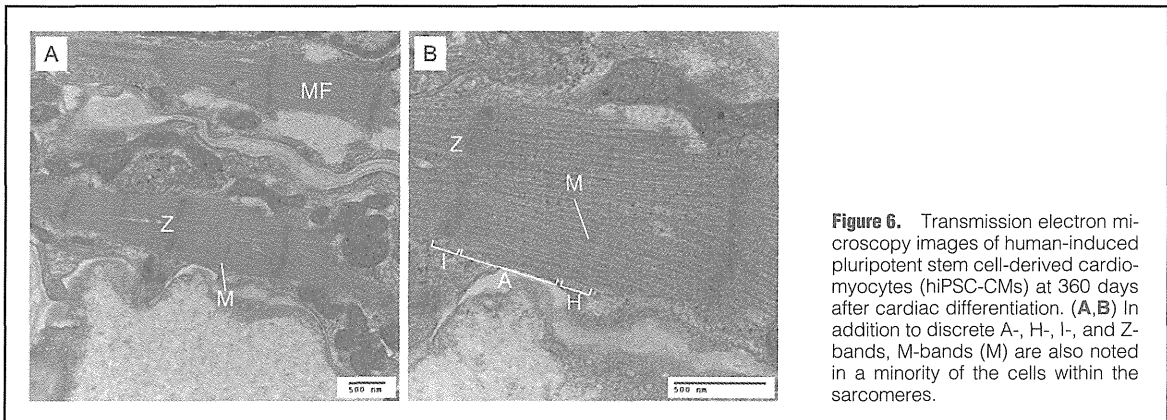

Figure 6. Transmission electron microscopy images of human-induced pluripotent stem cell-derived cardiomyocytes (hiPSC-CMs) at 360 days after cardiac differentiation. (**A,B**) In addition to discrete A-, H-, I-, and Z-bands, M-bands (M) are also noted in a minority of the cells within the sarcomeres.

noted in which myofibrils were held between a few of the Z-bands (Figure 3). However, A-, H-, I-, and M-bands were not recognized. CMs were connected by desmosomes and fascia adherens at this early stage.

At 30-day differentiation, nascent myofibrils decreased and appeared to be packed between Z-bands. Parallel Z-bands were demonstrated to confine the myofibrils in the typical sarcomeric pattern. Some myofibrils showed A- and I-bands. However, they still lacked the formation of H-, and M-bands (Figure 4). Mitochondria and rough endoplasmic reticulum were also noted, as previously reported.[13]

Between 60- and 90-day differentiation, ultrastructural maturation continued and formation of H-bands could be observed. However, even at 180-day differentiation, M-bands could not be detected (Figure 5).

Finally, at 360-day differentiation, in addition to discrete A-, H-, I-, and Z-bands, M-bands were first noted in a minority of the cells within the sarcomeres (Figure 6). Myofibrils appeared to be tightly packed and distributed in an oriented fashion. The amount of sarcomeric structure in a single CM continued to increase, but was still scarce compared with an adult CM. Even at this stage, different degrees of organization
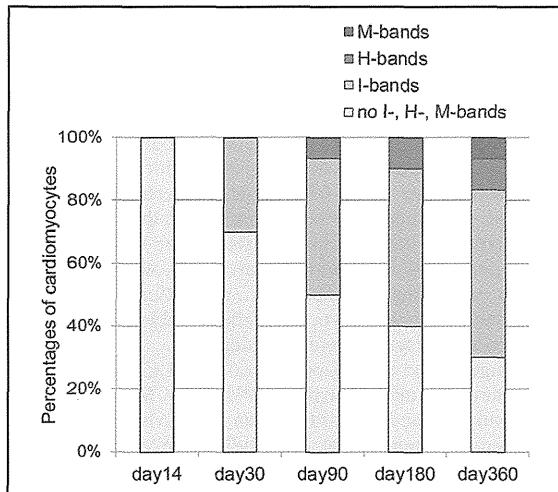
Figure 7. Percentages of the cardiomyocytes (CMs) having I-, H-, and M-bands at 14, 30, 90, 180, 360 days after cardiac differentiation. The amount of CMs with I- and H-bands increased through the long-term culture and M-bands were first noted in 360-day CMs.

existed simultaneously in the same EB.

We evaluated 30 CMs with sarcomeres on randomly selected electron micrographs to assess the maturation process of sarcomeres quantitatively. Figure 7 shows the percentages of CMs having I-, H-, and M-bands at 14-, 30-, 90-, 180-, 360-day differentiation.

Expression of Cardiac-Specific Genes

Leucine-rich repeat-containing protein 39 (LRRC39), myomesin 1 (MYOM1), and 2 (MYOM2), components of M-bands,[18] increased at 360-day differentiation compared with 30-day differentiation, supporting the observation of M-band formation in 360-day hiPSC-CMs (Figure 8). However, the expression levels of the M-band-specific proteins in the hiPSC-CMs were lower compared with those of the adult heart. The expression of cardiac troponin-T (cTnT), myosin heavy chain 6 (MYH6), myosin heavy chain 7 (MYH7), and myosin regulatory light chain 2 (MYL2) also increased after the 1-year culture. However, the expression levels of cardiac-specific genes in the hiPSC-CMs were also considerably lower than those in the adult heart left ventricle or left atrium, and in the fetal heart. The expression levels of gap junction α-1 protein were significantly decreased in 180-day and 360-day hiPSC-CMs compared with 30-day hiPSC-CMs.
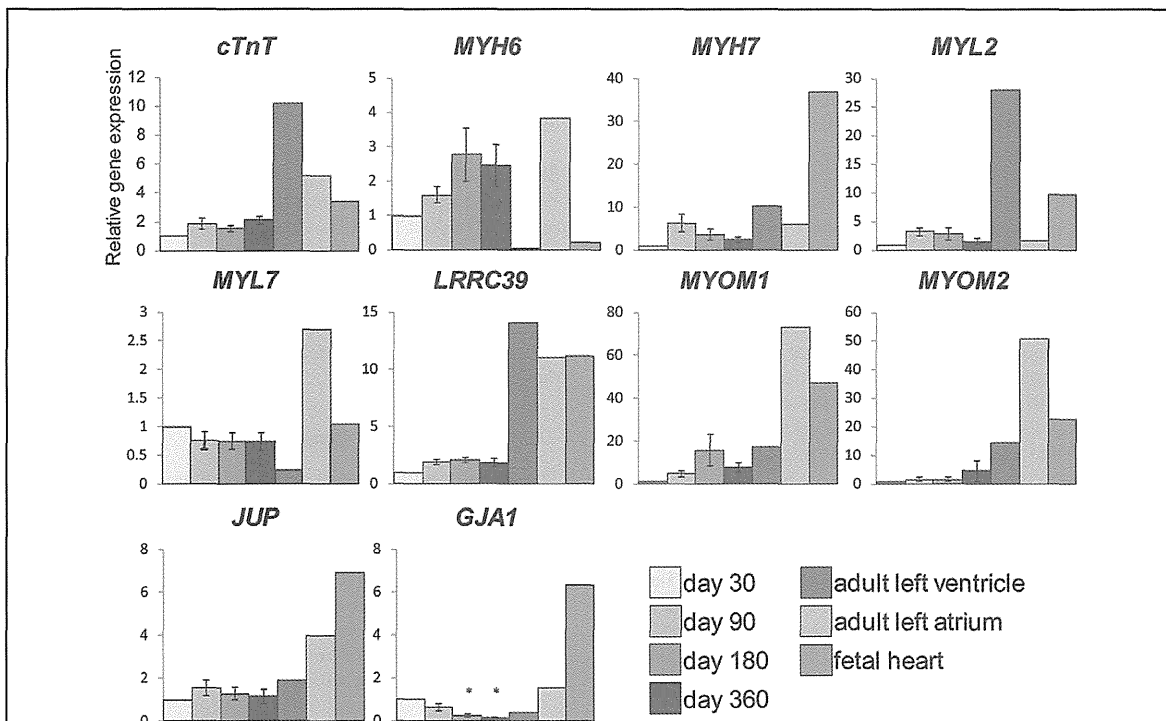
Figure 8. Real-time quantitative polymerase chain reaction analyses for cTnT, MYH6, MYH7, MYL2, MYL7, LRRC39, MYOM1, MYOM2, JUP, and GJA1 expression in beating embryoid bodies (EB) from human-induced pluripotent stem cell-derived cardiomyocytes (hiPSC-CMs) at 30, 90, 180, and 360 days, in the adult left ventricle, adult left atrium, and fetal heart. The changes in gene expression levels were compared with those of hiPSC-CMs at 30-day differentiation. cTnT, cardiac troponin-T; MYH6, myosin heavy chain 6; MYH7, myosin heavy chain 7; MYL2, myosin regulatory light chain 2; MYL7, myosin regulatory light chain 7; LRRC39, leucine-rich repeat-containing protein 39; MYOM1, myomesin 1; MYOM2, myomesin 2; JUP, junction plakoglobin; GJA1, gap junction α-1 protein. *P<0.05 vs. 30-days EBs.

Discussion

In this study, we demonstrated that hiPSC-CMs continue to mature through a 1-year culture. This is the first report of the feasibility of 1-year 2D culture of hiPSC-CMs and description of the sarcomeric maturation process represented by the emergence of M-bands and the increase in the cardiac-specific gene expressions.

So far, the reported ultrastructure of hiPSC-CMs has been immature and their maturation process remained unknown.[4,13,14] Human embryonic stem cell-derived cardiomyocytes (hESC-CMs) are reported to follow a roughly similar maturation process to that reported both in vivo and in an in-vitro murine ES model.[19–24] The hiPSC-CMs in the present study showed a similar maturation process to that of hESC-CMs.[25] At first, narrow, diffusely distributed, and frequently not well aligned myofibrils, resembling those of hiPSC-CMs at 14 days, developed into sarcomeres with clear band patterns including the Z-, I-, and A-bands, responding to hiPSC-CMs at between 30 and 90 days, and ultimately resulted in the generation of well-designed sarcomeres with A-, H-, I-, and M-bands. The ultrastructural findings of hiPSC-CMs in the literature now available relate to around 30 days of differentiation, and only Z- and I-bands have been visible.[4,13,14] In our study, the 30-day hiPSC-CMs similarly showed only Z- and I-bands, not H- or M-bands. Notably, we are the first to find that only 360-day hiPSC-CMs, not 180-day hiPSC-CMs, show a mature sarcomeric structure with M-bands. However, even at 360-day differentiation, different degrees of organization patterns existed simultaneously in the same EB and homogeneous maturation was not confirmed. Our 1-year culture system was able to confirm more mature sarcomeric structures than previously reported, but still not that of adult CMs. It is reported that human CMs derived from fetal hearts do not achieve full ultrastructural maturity and that myofibrillar development continues throughout the entire fetal period.[22] The insufficient maturation of hiPSC-CMs after long-term culture could be explained by several factors. In vitro culturing conditions lack the presence of adjacent non-myocyte proliferating cells, which play an important role in the maturation of CMs via paracrine and humoral signals in vivo. In addition, the CMs grown in the absence of hemodynamic workload typical of in vivo working CMs are reported to lack appropriate ultrastructural development.[26] The differences between in vitro and in vivo conditions, such as the absence of humoral factors and organized mechanical and electrical stress in vitro, might result in delayed ultrastructural maturation.

In electron micrographs of the sarcomere, the M-band appears as a series of parallel electron-dense lines in the central zone of the A-band. The M-band has been reported to play a role not only in mechanical stability in the activated sarcomere, such as reducing the intrinsic instability of thick filaments and helping titin to maintain order in sarcomeres, but also in the biomechanical conditions in contracting muscle such as stress sensing.[27] M-band formation was confirmed in the latest stage and has been considered the endpoint of myofibrillar maturation.[18,21] The lower expression levels of the M-band-specific proteins in the hiPSC-CMs compared with the adult heart might be associated with the delayed appearance of M-bands. Maturation of iPSC-CMs is critical for their application in regenerative medicine, as well as for investigating the mechanisms underlying inherited cardiac diseases. Techniques to promote the maturation of ESC-CMs, such as 3D culture methodology,[28] electric stimulation,[29] and coculture with non-cardiomyocytes[30] may be applicable to iPSC-

CMs to overcome the problem, although it has not been fully investigated in hiPSC-CMs. Improved methods are needed to produce homogeneous, mature iPSC-CMs.

In addition to ultrastructural maturation, there was a significant increase in the size of hiPSC-CMs after long-term culture, supporting the process of morphological maturation. Also, the lower rate of beating of 360-day hiPSC-CMs compared with 30-day hiPSC-CMs suggested electrophysiological maturation, because it has been reported that the resting membrane potential becomes progressively more negative in the developing atrial and ventricular myocytes, which correlates with an increasing presence of I_{K1}, and ultimately, the fetal atrial and ventricular myocytes exhibit stable resting membrane potentials with little automaticity.[31]

Changes in the expression patterns of MLC2v and MLC2a occur during the maturation process.[32] hiPSC-CMs were thought to be immature and similar to human fetal CMs because of the presence of a number of MLC2v/MLC2a double-positive CMs.[33] Our immunostaining analysis demonstrated that the percentage of MLC2v/MLC2a double-positive hiPSC-CMs decreased after long-term culture, accompanied by an increase in MLC2v-positive/MLC2a-negative hiPSC-CMs, suggesting maturing of the ventricular-type CMs.

This study also showed for the first time, changes in the expression levels of cardiac-specific genes and genes related to intercalated discs throughout the 1-year culture. The cardiac-specific genes tended to increase during 1-year culture, supporting the maturation process of hiPSC-CMs. The connexin (gap junction proteins) are reported to be more abundant in the neonate than the adult.[34] The significant decrease in *GJA1* expression levels in 180- and 360-day hiPSC-CMs compared with 30-day hiPSC-CMs also suggested maturation of hiPSC-CMs.

Study Limitations
We used microdissected beating EBs for the gene expression studies. The fact that EBs contain CMs at various stages of differentiation, as well as non-CMs, might obscure the results of the gene expression studies. We conducted immunostaining analysis of single cells from microdissected beating EBs 3 days after enzymatic dispersion, which might allow non-CMs to increase and affect the results of the percentage of CMs in the beating EBs.

Conclusions

The current study demonstrated developmental changes in the ultrastructural, immunocytological, and gene expression properties of hiPSC-CMs. Our results confirmed mature sarcomeric structure with M-band formation in long-term culture of hiPSC-CMs for the first time, which provides a new insight into the maturation process of hiPSC-CMs. For application of homogeneous mature hiPSC-CMs in regenerative medicine and in vitro modeling of human cardiac diseases, further maturation of cardiac cells will be needed.

References

1. Takahashi K, Tanabe K, Ohnuki M, Narita M, Ichisaka T, Tomoda K, et al. Induction of pluripotent stem cells from adult human fibroblasts by defined factors. *Cell* 2007; **131:** 861–872.
2. Zhang J, Wilson GF, Soerens AG, Koonce CH, Yu J, Palecek SP, et al. Functional cardiomyocytes derived from human-induced pluripotent stem cells. *Circ Res* 2009; **104:** e30–e41.
3. Moretti A, Bellin M, Welling A, Jung CB, Lam JT, Bott-Flügel L, et al. Patient-specific induced pluripotent stem-cell models for long-QT syndrome. *N Engl J Med* 2010; **363:** 1397–1409.
4. Novak A, Barad L, Zeevi-Levin N, Shick R, Shtrichman R, Lorber A, et al. Cardiomyocytes generated from CPVT^D307H patients are arrhythmogenic in response to β-adrenergic stimulation. *J Cell Mol Med* 2012; **16:** 468–482.
5. Choi SH, Jung SY, Kwon SM, Baek SH. Perspectives on stem cell therapy for cardiac regeneration. *Circ J* 2012; **76:** 1307–1312.
6. Zwi L, Caspi O, Arbel G, Huber I, Gepstein A, Park IH, et al. Cardiomyocyte differentiation of human-induced pluripotent stem cells. *Circulation* 2009; **120:** 1513–1523.
7. Germanguz I, Sedan O, Zeevi-Levin N, Shtrichman R, Barak E, Ziskind A, et al. Molecular characterization and functional properties of cardiomyocytes derived from human inducible pluripotent stem cells. *J Cell Mol Med* 2011; **14:** 38–51.
8. Ma J, Guo L, Fiene SJ, Anson BD, Thomson JA, Kamp TJ, et al. High purity human-induced pluripotent stem cell-derived cardiomyocytes electrophysiological properties of action potentials and ionic currents. *Am J Physiol Heart Circ Physiol* 2011; **301:** H2006–H2017.
9. Tanaka T, Tohyama S, Murata M, Nomura F, Kaneko T, Chen H, et al. In vitro pharmacologic testing using human-induced pluripotent stem cell-derived cardiomyocytes. *Biochem Biophys Res Commun* 2009; **385:** 497–502.
10. Xi J, Khalil M, Shishechian N, Hannes T, Pfannkuche K, Liang H, et al. Comparison of contractile behavior of native murine ventricular tissue and cardiomyocytes derived from embryonic or induced pluripotent stem cells. *FASEB J* 2010; **24:** 2739–2751.
11. Kuzmenkin A, Liang H, Xu G, Pfannkuche K, Eichhorn H, Fatima A, et al. Functional characterization of cardiomyocytes derived from murine induced pluripotent stem cells in vitro. *FASEB J* 2009; **23:** 4168–4180.
12. Jonsson MK, Vos MA, Mirams GR, Duker G, Sartipy P, de Boer TP, et al. Application of human stem cell-derived cardiomyocytes in safety pharmacology requires caution beyond hERG. *J Mol Cell Cardiol* 2012; **52:** 998–1008.
13. Gherghiceanu M, Barad L, Novak A, Reiter I, Itskovitz-Eldor J, Binah O, et al. Cardiomyocytes derived from human embryonic and induced pluripotent stem cells: Comparative ultrastructure. *J Cell Mol Med* 2011; **15:** 2539–2551.
14. Fujiwara M, Yan P, Otsuji TG, Narazaki G, Uosaki H, Fukushima H, et al. Induction and enhancement of cardiac cell differentiation from mouse and human-induced pluripotent stem cells with cyclosporine-A. *PLoS One* 2011; **6:** e16734.
15. Yoshida Y, Takahashi K, Okita K, Ichisaka T, Yamanaka S. Hypoxia enhances the generation of induced pluripotent stem cells. *Cell Stem Cell* 2009; **5:** 237–241.
16. Dubois NC, Craft AM, Sharma P, Elliott DA, Stanley EG, Elefanty AG, et al. SIRPA is a specific cell-surface marker for isolating cardiomyocytes derived from human pluripotent stem cells. *Nat Biotechnol* 2011; **29:** 1011–1018.
17. Yang L, Soonpaa MH, Adler ED, Roepke TK, Kattman SJ, Kennedy M, et al. Human cardiovascular progenitor cells develop from a KDR+ embryonic-stem-cell-derived population. *Nature* 2008; **453:** 524–528.
18. Will RD, Eden M, Just S, Hansen A, Eder A, Frank D, et al. Myomasp/LRRC39, a heart- and muscle-specific protein, is a novel component of the sarcomeric M-band and is involved in stretch sensing. *Circ Res* 2010; **107:** 1253–1264.
19. Beharvand H, Azarnia M, Parivar K, Ashtiani SK. The effect of extracellular matrix on embryonic stem cell-derived cardiomyocytes. *J Mol Cel Cardiol* 2005; **38:** 495–503.
20. Baharvand H, Piryaei A, Rohani R, Taei A, Heidari MH, Hosseini A. Ultrastructural comparison of developing mouse embryonic stem cell- and in vivo-derived cardiomyocytes. *Cell Biol Int* 2006; **30:** 800–807.
21. Anversa P, Olivetti G, Bracchi PG, Loud AV. Postnatal development of the M-band in rat cardiac myofibrils. *Circ Res* 1981; **48:** 561–568.
22. Kim HD, Kim DJ, Lee IJ, Rah BJ, Sawa Y, Schaper J. Human fetal heart development after mid-term: Morphometry and ultrastructural study. *J Mol Cell Cardiol* 1992; **24:** 949–965.
23. Legat MJ. Sarcomerogenesis in human myocardium. *J Mol Cell Cardiol* 1970; **1:** 425–437.
24. Yu L, Gao S, Nie L, Tang M, Huang W, Luo H, et al. Molecular and functional changes in voltage-gated Na+ channels in cardiomyocytes during mouse embryogenesis. *Circ J* 2011; **75:** 2071–2079.
25. Snir M, Kehat I, Gepstein A, Coleman R, Itskovitz-Eldor J, Livne E, et al. Assessment of the ultrastructural and proliferative properties of human embryonic stem cell-derived cardiomyocytes. *Am J Physiol Heart Circ Physiol* 2003; **285:** H2355–H2363.
26. Bishop SP, Anderson PG, and Tucker DC. Morphological development of the rat heart growing in oculo in the absence of hemodynamic work load. *Circ Res* 1990; **66:** 84–102.
27. Agarkova I, Perriard JC. The M-band: An elastic web that crosslinks thick filaments in the center of the sarcomere. *Trends Cell Biol* 2005; **15:** 477–485.
28. Ou DB, He Y, Chen R, Teng JW, Wang HT, Zeng D, et al. Three-dimensional co-culture facilitates the differentiation of embryonic stem cells into mature cardiomyocytes. *J Cell Biochem* 2011; **112:** 3555–3562.
29. Chen MQ, Xie X, Wilson KD, Sun N, Wu JC, Giovangrandi L, et al. Current-controlled electrical point-source stimulation of embryonic stem cells. *Cell Mol Bioeng* 2009; **2:** 625–635.
30. Kim C, Majdi M, Xia P, Wei KA, Talantova M, Spiering S, et al. Non-cardiomyocytes influence the electrophysiological maturation of human embryonic stem cell-derived cardiomyocytes during differentiation. *Stem Cells Dev* 2010; **19:** 783–795.
31. He JQ, Ma Y, Lee Y, Thomson JA, Kamp TJ. Human embryonic stem cells develop into multiple types of cardiac myocytes: Action potential characterization. *Circ Res* 2003; **93:** 32–39.
32. Kubalak SW, Miller-Hance WC, O'Brien TX, Dyson E, Chien KR. Chamber specification of atrial myosin light chain-2 expression precedes septation during murine cardiogenesis. *J Biol Chem* 1994; **269:** 16961–16970.
33. Mummery CL, Zhang J, Ng ES, Elliott DA, Elefanty AG, Kamp TJ. Differentiation of human embryonic stem cells and induced pluripotent stem cells to cardiomyocytes: A methods overview. *Circ Res* 2012; **111:** 344–358.
34. Allah EA, Tellez JO, Yanni J, Nelson T, Monfredi O, Boyett MR, et al. Changes in the expression of ion channels, connexins and Ca2+-handling proteins in the sino-atrial node during postnatal development. *Exp Physiol* 2011; **96:** 426–438.

Supplementary Files

Supplementary File 1

Table S1. Primer Sequences Used for Real-Time qPCR Analysis

Supplementary File 2

Movie S1. 360-day-old beating embryoid bodies.

Please find supplementary file(s);
http://dx.doi.org/10.1253/circj.CJ-12-0987

Novel *SCN3B* Mutation Associated With Brugada Syndrome Affects Intracellular Trafficking and Function of Nav1.5

Taisuke Ishikawa, BSc; Naohiko Takahashi, MD; Seiko Ohno, MD; Harumizu Sakurada, MD;
Kazufumi Nakamura, MD; Young Keun On, MD; Jeong Euy Park, MD; Takeru Makiyama, MD;
Minoru Horie, MD; Takuro Arimura, PhD; Naomasa Makita, MD; Akinori Kimura, MD

Background: Brugada syndrome (BrS) is characterized by specific alterations on ECG in the right precordial leads and associated with ventricular arrhythmia that may manifest as syncope or sudden cardiac death. The major causes of BrS are mutations in *SCN5A* for a large subunit of the sodium channel, Nav1.5, but a mutation in *SCN3B* for a small subunit of sodium channel, Navβ3, has been recently reported in an American patient.

Methods and Results: A total of 181 unrelated BrS patients, 178 Japanese and 3 Koreans, who had no mutations in *SCN5A*, were examined for mutations in *SCN3B* by direct sequencing of all exons and adjacent introns. A mutation, Val110Ile, was identified in 3 of 178 (1.7%) Japanese patients, but was not found in 480 Japanese controls. The *SCN3B* mutation impaired the cytoplasmic trafficking of Nav1.5, the cell surface expression of which was decreased in transfected cells. Whole-cell patch clamp recordings of the transfected cells revealed that the sodium currents were significantly reduced by the *SCN3B* mutation.

Conclusions: The Val110Ile mutation of *SCN3B* is a relatively common cause of *SCN5A*-negative BrS in Japan, which has a reduced sodium current because of the loss of cell surface expression of Nav1.5. (*Circ J* 2013; **77:** 959–967)

Key Words: Brugada syndrome; Electrophysiologic study; Genetics; Ion channels; Sodium

Brugada syndrome (BrS) is a cardiac channelopathy characterized by specific findings, such as accentuated J wave and ST-segment elevation in the right precordial leads on ECG, in the absence of structural heart diseases.[1–3] BrS patients sometimes suffer from syncope, and have a risk of sudden cardiac death caused by rapid polymorphic ventricular tachycardia or ventricular fibrillation.[1–3] Approximately 35% of BrS patients have a family history of the disease, which is consistent with the autosomal dominant inheritance, and mutations in 12 different genes have been reported as associated with BrS, of which the majority are mutations in *SCN5A* encoding a large subunit of the cardiac sodium channel Nav1.5.[3–12] The prevalence of BrS in East Asia including Japan is much higher, reaching 1 in 1,000–2,000, than the worldwide prevalence of approximately 1 in 10,000.[13–15]

Editorial p 900

In cardiomyocytes, 5 distinct sodium channel β-subunits, Navβ1, Navβ1b, β2, β3 and β4, are known to be expressed. In particular, Navβ1 and Navβ3, encoded by *SCN1B* and *SCN3B*, are abundantly expressed, and these auxiliary β-subunits and a pore-forming subunit, Nav1.5, comprise the cardiac sodium channel complex.[4,16] Inward sodium current (I_{Na}) generated by the sodium channel complex is crucial for the cardiac action potential,[16,17] and functional alterations of I_{Na} caused by gene mutations have been reported in a wide range of arrhythmias, including long QT syndrome,[18] idiopathic ventricular fibrillation (IVF),[19] sudden infant death syndrome (SIDS),[20] and atrial fibrillation (AF).[21] In BrS patients, disease-causing mutations were found not only in *SCN5A* but also in the genes
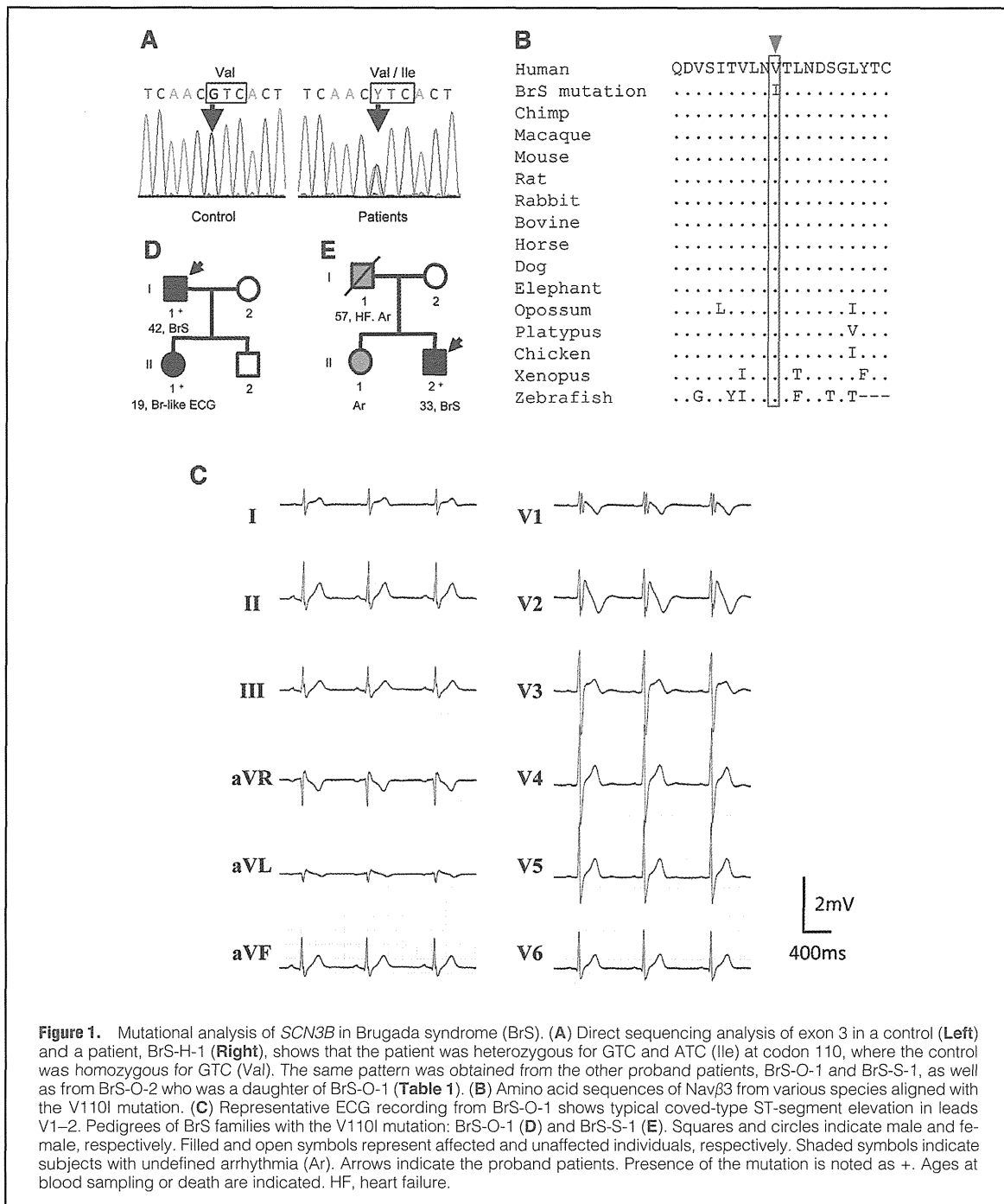
Figure 1. Mutational analysis of *SCN3B* in Brugada syndrome (BrS). (**A**) Direct sequencing analysis of exon 3 in a control (**Left**) and a patient, BrS-H-1 (**Right**), shows that the patient was heterozygous for GTC and ATC (Ile) at codon 110, where the control was homozygous for GTC (Val). The same pattern was obtained from the other proband patients, BrS-O-1 and BrS-S-1, as well as from BrS-O-2 who was a daughter of BrS-O-1 (**Table 1**). (**B**) Amino acid sequences of Navβ3 from various species aligned with the V110I mutation. (**C**) Representative ECG recording from BrS-O-1 shows typical coved-type ST-segment elevation in leads V1–2. Pedigrees of BrS families with the V110I mutation: BrS-O-1 (**D**) and BrS-S-1 (**E**). Squares and circles indicate male and female, respectively. Filled and open symbols represent affected and unaffected individuals, respectively. Shaded symbols indicate subjects with undefined arrhythmia (Ar). Arrows indicate the proband patients. Presence of the mutation is noted as +. Ages at blood sampling or death are indicated. HF, heart failure.

encoding modifier proteins of Nav1.5, which causes functional loss of I_{Na}.[8,12,22–25] Among the modifier proteins, Navβ3, which does not form the ion-conducting pore, modifies the function of Nav1.5 by modulating channel gating and increasing the cell surface expression of Nav1.5,[26] and hence *SCN3B* mutations could be responsible for BrS. Nevertheless, there is only 1 report of a *SCN3B* mutation, Leu10Pro, in an American patient with BrS,[23] although some other *SCN3B* mutations have been reported in other hereditary arrhythmias, including IVF,[27] SIDS,[28] and AF.[29,30]

We report a *SCN3B* mutation, Val110Ile, found in 3 unrelated Japanese BrS patients. Functional studies in transfected cells demonstrated that the mutation decreased the cell surface expression of Nav1.5 and reduced the peak current of the I_{Na}.

ID	Age (years)/Sex	ST-elevation type	Symptoms	Family history of arrhythmia/SCD	ICD	EPS
BrS-O-1	42/M	Coved	Symptomatic	Yes	Yes	VF
BrS-O-2	19/F	Coved	Asymptomatic	Yes	No	–
BrS-S-1	33/M	Saddleback	Asymptomatic	Yes	No	NSVT
BrS-H-1	51/M	Coved	Syncope	No	No	–

Table 1. Clinical Phenotypes of Individuals Carrying the *SCN3B* Val110Ile Mutation

BrS, Brugada syndrome; EPS, electrophysiologic study; ICD, implantable cardioverter defibrillator; NSVT, non-sustained ventricular tachycardia; SCD, sudden cardiac death; VF, ventricular fibrillation.

Methods

Subjects
We studied 178 genetically unrelated Japanese and 3 Korean patients with BrS. Age at the diagnosis of 145 male patients was 45.3±15.7 (range 7–76) years, and that of the 17 female patients was 46.8±17.3 (range 11–72) years. Episodes of syncope and/or arrhythmia had occurred in 93 patients, but the others were asymptomatic. There was a family history of sudden death and/or arrhythmias for 19 patients, but nothing certain for the others. Blood samples were obtained from each subject after informed consent for gene analysis was given. The patients had been analyzed for mutations in *SCN5A* by using specific primer pairs (Table S1), and no disease-related mutation was found. The control subjects were 480 genetically unrelated Japanese individuals who were selected at random without ECG records.

The research protocol was approved by the Ethics Review Committee of the Medical Research Institute, Tokyo Medical and Dental University and the Institutional Review Board of Samsung Medical Center.

Mutational Analysis
Genomic DNA extracted from the peripheral blood leukocytes of each individual was subjected to polymerase chain reaction (PCR) using primer pairs specific to *SCN3B* (Table S2). PCR products were analyzed for mutations by direct DNA sequencing using Big Dye Terminator version 3.1 and ABI3100 DNA analyzer (Applied Biosystems, Foster City, CA, USA). The proband patients carrying the Val110Ile mutation were analyzed for mutations in the other known BrS susceptibility genes, *CACNA1C, CACNB2, GPD1-L, KCNJ8, SCN1B, KCNE3, MOG1, HCN4, KCND3* and *KCNE5*, by sequencing of PCR products amplified with specific primer pairs (Table S1).

Alignment of Amino Acid Sequences
Amino acid sequences of human Navβ3 protein predicted from the nucleotide sequences (GenBank™ NM_018400) were aligned with those of chimpanzee (XM_522210), macaque (NM_001194283), mouse (NM_153522), rat (NM_139097), rabbit (ENSOCUP00000009050), bovine (NM_001046495), horse (ENSECAT00000025763), dog (XM_847682), elephant (ENSLAFT00000000307), opossum (XM_001379934), platypus (ENSOANT00000023925), chicken (XM_417884), *Xenopus* (NM_001011299), and zebrafish (NM_001080802).

Constructs for Nav1.5 and Navβ3
We obtained a cDNA fragment of human Navβ3 by reverse transcription-PCR from human adult heart cDNA. Mutant cDNA fragments of Navβ3 containing a T to C substitution in codon 10 (for Leu10Pro mutation) or a G to A substitution at codon 110 (for Val110Ile mutation) were created by the primer-mediated mutagenesis method using specific primers (Table S3). Wild-type (WT) or mutant cDNA fragments were cloned into pcDNA3.1-myc, His-B (myc-His-Navβ3) (Invitrogen, San Diego, CA, USA) and pIRES-CD8 (pIRES-CD8-Navβ3). The cDNA fragment of human *SCN5A* was a gift from Dr A.L. George (Vanderbilt University). A Flag-tagged Nav1.5 was constructed by inserting a Flag epitope (DYKDDDDK) into the extracellular linker 1 (L1) between S1 and S2 in the D1 domain after position aa154 in the Nav1.5 construct (L1-Flag-Nav1.5), as described previously.[18] All constructs were sequenced to ensure that no errors were introduced.

Immunofluorescence Microscopy
We seeded 4.0×10^4 tsA-201 cells, a derivative line of HEK cells, onto poly-D-Lysine 8-well culture slides (BD Biosciences, San Jose, CA, USA), and 24h later, myc-His-Navβ3 (0.1 μg) alone, or L1-Flag-Nav1.5 (0.1 μg) plus myc-His-Navβ3 (0.1 μg) were added to the wells with Lipofectamine 2000 Reagent (Invitrogen) (0.2 or 0.4 μl, respectively). After 18h, the cells were washed with phosphate-buffered saline (PBS), fixed in 4% paraformaldehyde for 15min at room temperature and permeabilized by 0.15% Triton X-100 in PBS with 3% bovine serum for 20min at room temperature. The cells were then incubated with the primary rabbit anti-Flag polyclonal antibody (Ab) (1:250, Sigma, CA, USA) and mouse anti-myc monoclonal Ab (1:200, Santa Cruz Biotechnology, Santa Cruz, CA, USA), and secondary Alexa Fluor 568 goat anti-rabbit IgG (1:500, Molecular Probes, Eugene, OR, USA) and Alexa Fluor 488 rabbit anti-mouse IgG (1:1,000, Molecular Probes), respectively, in PBS with 3% bovine serum. All cells were mounted on glass slides using Mowiol 4-88 Reagent (Calbiochem, Darmstadt, Germany), and images were collected and analyzed with an LSM510 laser-scanning microscope (Carl Zeiss Microscopy, Jena, Germany). To quantify the membrane expression of Nav1.5, fluorescence intensity of the total cell and the plasma membrane (peripheral, 2 μm) areas in the middle *xy* images of *z* series stack were measured, and the ratios of peripheral to total cell area fluorescence intensity (PTAFI) were calculated as described previously.[23] Analyses of labeled cells were performed using ImageJ software (NIH, MD, USA).[31]

Electrophysiological Studies
The tsA-201 cell line was used in the electrophysiological study, as described previously.[18] Cells transfected with pIRES-CD8 or pIRES-CD8-Navβ3 were briefly preincubated with Dynabeads M-450 CD8 (Dynal, Oslo, Norway) prior to the recordings. Sodium currents were recorded from the cells that were labeled with Dynabeads using the whole-cell patch clamp technique. Currents and cell capacitances were recorded using Axopatch 200B amplifier (Axon Instruments, CA, USA) and series resistance errors were reduced by 60–70% using elec-
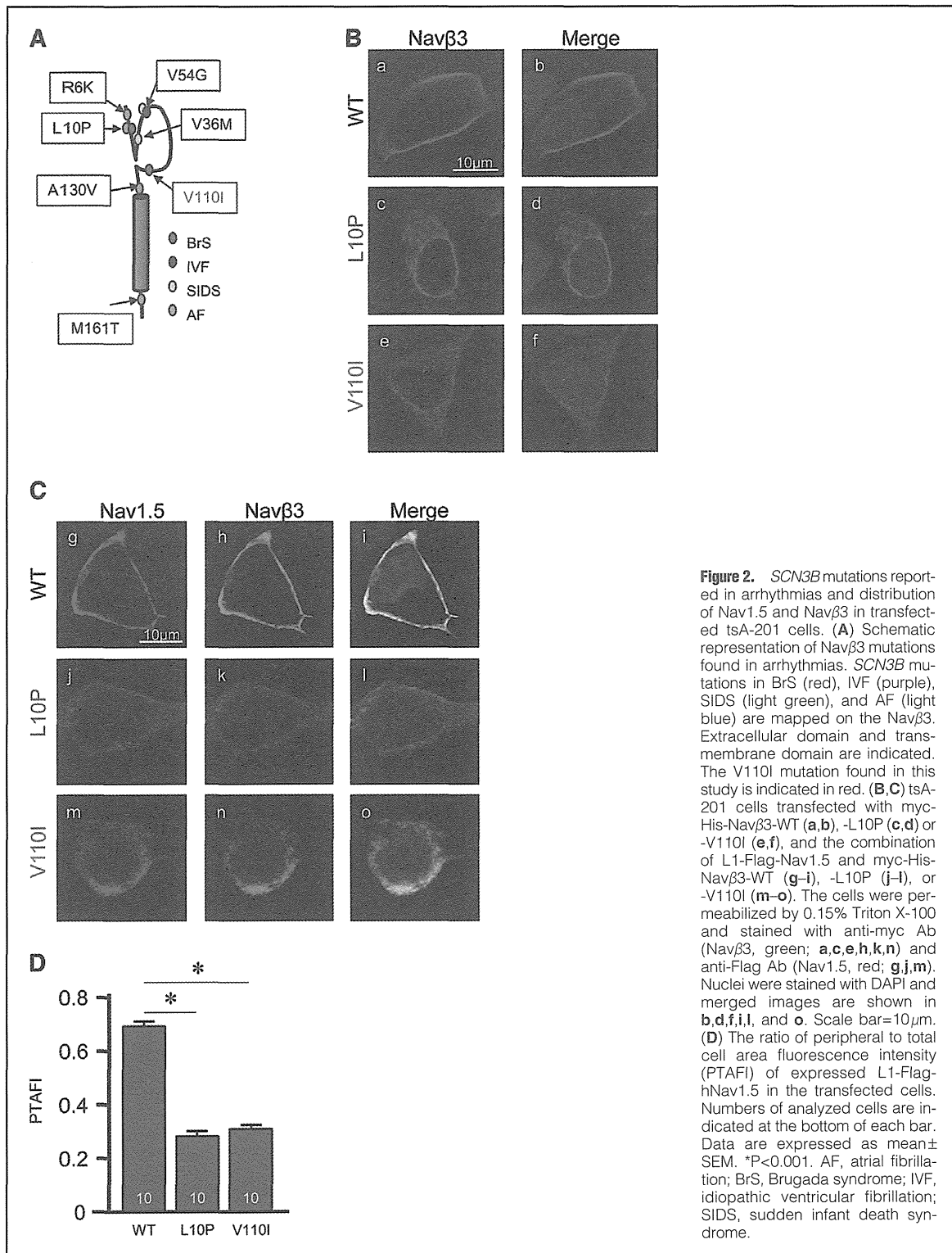
Figure 2. *SCN3B* mutations reported in arrhythmias and distribution of Nav1.5 and Navβ3 in transfected tsA-201 cells. (**A**) Schematic representation of Navβ3 mutations found in arrhythmias. *SCN3B* mutations in BrS (red), IVF (purple), SIDS (light green), and AF (light blue) are mapped on the Navβ3. Extracellular domain and transmembrane domain are indicated. The V110I mutation found in this study is indicated in red. (**B,C**) tsA-201 cells transfected with myc-His-Navβ3-WT (**a,b**), -L10P (**c,d**) or -V110I (**e,f**), and the combination of L1-Flag-Nav1.5 and myc-His-Navβ3-WT (**g–i**), -L10P (**j–l**), or -V110I (**m–o**). The cells were permeabilized by 0.15% Triton X-100 and stained with anti-myc Ab (Navβ3, green; **a,c,e,h,k,n**) and anti-Flag Ab (Nav1.5, red; **g,j,m**). Nuclei were stained with DAPI and merged images are shown in **b,d,f,i,l**, and **o**. Scale bar=10μm. (**D**) The ratio of peripheral to total cell area fluorescence intensity (PTAFI) of expressed L1-Flag-hNav1.5 in the transfected cells. Numbers of analyzed cells are indicated at the bottom of each bar. Data are expressed as mean± SEM. *P<0.001. AF, atrial fibrillation; BrS, Brugada syndrome; IVF, idiopathic ventricular fibrillation; SIDS, sudden infant death syndrome.

Table 2. Kinetics of I_{Na} in Transfected tsA-201 Cells

Transfected constructs	Peak I_{Na} (at –25 mV)		Activation			Inactivation			Recovery	
	pA/pF	n	$V_{1/2}$ (mV)	κ	n	$V_{1/2}$ (mV)	κ	n	Time required for e^{-1} fraction recovery (ms)	n
SCN5A without SCN3B	–59.83±11.36**	10	–35.23±1.83*	–7.49±0.29*	10	–78.66±1.59*	7.63±0.29*	10	10.29±0.81**	9
SCN5A+SCN3B-WT	–110.28±8.92	11	–43.22±2.11	–6.68±0.21	11	–82.40±1.96	6.83±0.15	11	6.06±1.10	9
SCN5A+SCN3B-L10P	–68.09±5.81**	13	–40.39±1.98	–6.51±0.17	13	–83.49±1.10	6.40±0.23	11	8.88±0.99**	10
SCN5A+SCN3B-V110I	–62.72±5.10**	15	–40.28±1.82	–6.35±0.12	15	–81.98±1.34	6.60±0.18	15	6.10±0.92	12
SCN5A+SCN3B-WT/L10P	–82.46±8.21*	13	–41.49±2.01	–6.27±0.19	13	–81.76±1.49	6.59±0.27	13	6.87±1.00	12
SCN5A+SCN3B-WT/V110I	–77.77±7.31**	13	–41.57±1.45	–6.16±0.26	13	–81.17±1.03	6.44±0.13	12	6.44±1.45	12

*$P<0.05$ vs. SCN5A+SCN3B-WT, **$P<0.01$ vs. SCN5A+SCN3B-WT.
I_{Na}, inward sodium current; WT, wild-type.

tronic compensation. Holding potentials were –120 mV and pipette resistance was 1.0–1.5 MΩ. The bath solution contained 36 mmol/L NaCl, 109 mmol/L NMG, 4 mmol/L KCl, 1.8 mmol/L $CaCl_2$, 1 mmol/L $MgCl_2$, and 10 mmol/L HEPES, pH 7.35, while the pipette solution contained 10 mmol/L NaF, 110 mmol/L CsF, 20 mmol/L CsCl, 10 mmol/L EGTA, and 10 mmol/L HEPES, pH 7.35. All signals were acquired at 20–50 kHz (Digidata 1332, Axon Instruments) with a personal computer running Clampex 8 software (Axon Instruments) and filtered at 5 kHz with a 4-pole Bessel low-pass filter. Experiments were done at room temperature. Membrane currents were analyzed with Clampfit 8 software (Axon Instruments) and Sigmaplot (Systat Software, CA, USA). The current-voltage relationships were fit to the Boltzmann equation,

$$I = (V - V_{rev}) \times G_{max} \times [1 + \exp((V - V_{1/2})/\kappa)] - 1,$$

where I is the peak sodium current during the test pulse potential V. The parameters estimated by the fitting are V_{rev} (reversal potential), G_{max} (maximum conductance), and κ (slope factor). Steady-state availability was fit with the Boltzmann equation,

$$I/I_{max} = [1 + \exp((V - V_{1/2})/\kappa)] - 1,$$

where I_{max} is the maximum peak sodium current, to determine the membrane potential for $V_{1/2}$ (half-maximal inactivation) and κ (slope factor). The time course of inactivation was fit with a 2-exponential function,

$$I(t)/I_{max} = A0 + A1 \times \exp(-t/\tau_1) + A2 \times \exp(-t/\tau_2),$$

where A and τ are amplitudes and time constants, respectively. I and t refer to current and time, respectively.

Co-Immunoprecipitation (co-IP) Assay

The tsA-201 cells were transiently transfected with a combination of L1-Flag-Nav1.5 (2 μg) and myc-His-Navβ3 (2 μg). Cellular extracts were prepared from the transfected cells and equal amount of extracted proteins were used for the co-IP assay using the Catch and Release version 2.0 reversible immunoprecipitation system, according to the manufacturer's instructions (Millipore, Milford, MA, USA), with rabbit anti-Flag polyclonal Ab (Sigma). Eluted samples were separated by SDS-PAGE, transferred to a nitrocellulose membrane, pre-incubated with 5% skimmed milk in PBS, and incubated with primary mouse anti-c-myc monoclonal Ab (1:100) followed by secondary rabbit anti-mouse (for monoclonal Ab) IgG HRP-conjugated Ab (1:1,000; Dako A/S, Glostrup, Denmark).

Statistical Analysis

Numerical data are expressed as mean±SEM. Statistical dif-

ferences were analyzed using 1-way analysis of variance (ANOVA) followed by Dunnett's test. $P<0.05$ was considered to be statistically significant.

Results

Mutational Analysis of SCN3B

We analyzed 181 BrS patients, who were negative for *SCN5A* mutations, for sequence variations in *SCN3B* and found a synonymous and another non-synonymous variant in 1 and 3 patients, respectively. The synonymous variant, p.Asn113Asn (c.339C>T), was rare and was not considered to be a disease-causing mutation because no functional effect was deduced. On the other hand, the non-synonymous variant, p.Val110Ile (V110I, c.328G>A) (**Figure 1A**), was found in 3 unrelated Japanese patients; a 42-year-old male (BrS-O-1), a 33-year-old male (BrS-S-1), and a 51-year-old male (BrS-H-1) (**Table 1**). The V110I variant was predicted to affect an evolutionary conserved residue of Navβ3 (**Figure 1B**) and was not found in 960 control chromosomes. As summarized in **Table 1**, BrS-O-1 had experienced repetitive syncope, and showed spontaneous coved-type ST-elevation in ECG (**Figure 1C**). His daughter (BrS-O-2) was asymptomatic, but exhibited a BrS-like ECG pattern and carried the same mutation (**Table 1**, **Figure 1D**). BrS-S-1 was asymptomatic, showed saddleback-type ST-segment elevation, and pilsicainide administration converted the ST-segment elevation into the coved type. His father and sister had arrhythmia, although the details could not be evaluated (**Figure 1E**). BrS-H-1 had experienced syncope, and showed spontaneous coved-type ST-elevation in ECG, but the family history of arrhythmia was uncertain. These 3 proband patients were also analyzed for mutations in the other known disease genes for BrS (**Table S1**) and none had any mutation.

Cell Surface Expression of Nav1.5 in the Presence of Mutant Navβ3

Navβ3 modulates the function of the Nav1.5 channel, and several *SCN3B* mutations have been reported in association with arrhythmias, including BrS, IVF, SIDS, and AF (**Figure 2A**). Because the Leu10Pro (L10P) mutation was the only mutation previously reported in only 1 BrS patient, which resulted in the reduction of I_{Na} in transfected cells,[23] we investigated the functional alterations caused by the V110I mutation as compared with the L10P mutation. Membrane surface expression of Nav1.5 was examined in tsA-201 cells transfected with myc-His-Navβ3 alone or in combination with L1-Flag-Nav1.5. It was observed that Navβ3-WT was expressed on the cell